Reliability assessment of Ti/$TaSi_2$/Pt ohmic contacts on SiC after 1000 h at 600 °C

Robert S. Okojie[a)]
NASA Glenn Research Center, 21000 Brookpark Road, M/S 77-1, Cleveland, Ohio 44135

Dorothy Lukco and Yuanliang L. Chen
QSS, 21000 Brookpark Road, Mail Stop GEC-QSS, Cleveland, Ohio 44135

David J. Spry
OAI, 22800 Cedar Point Road, Cleveland, Ohio 44142

(Received 13 December 2001; accepted for publication 25 February 2002)

We report the result of the development and analysis of Ti/$TaSi_2$/Pt high temperature ohmic contact metallizations on *n*-type 4H– and 6H–SiC that can successfully withstand 1000 h of 600 °C thermal treatment in air. Understanding the reaction kinetics and dominant failure mechanisms enabled metal thicknesses in the multilayer stack to be optimized, thereby providing stable specific contact resistivity in the range of $1-6\times10^{-5}\ \Omega\,\mathrm{cm}^2$ on the *n*-type 4H–SiC and 6H–SiC epilayers throughout the duration of heat treatment in air. The deleterious effects of platinum in a platinum-rich silicide and the benefits in a platinum Si-rich silicide were identified within the multilayer system. A high temperature ohmic contact figure of merit is proposed as a reliability benchmark and calculated for the contacts to 4H– and 6H–SiC. [DOI: 10.1063/1.1470255]

I. INTRODUCTION

Semiconductor-based sensors and electronics targeted for insertion into high temperature, extreme vibration, and corrosive environments must satisfy new sets of minimum reliability criteria because the dominant failure mechanisms are not necessarily the same as in conventional devices that operate at lower temperatures. The reliability qualification of these devices will ultimately increase device acceptance for large-scale applications. The electrical and mechanical properties of wide band gap electronic materials at temperatures above 300 °C have long been recognized to be superior to conventional semiconductors such as silicon and gallium arsenide.[1] Substantial progress has been made in silicon carbide (SiC) based electronics and sensors, which should eventually enable their insertion into designated high temperature environments.[2] However, the improved precision instrumentation in harsh environments that SiC electronics and sensors promise cannot materialize until the fundamental reliability challenges that currently exist are overcome. The crucial need for thermally stable ohmic and Schottky contacts to these devices has been the subject of extensive research efforts with an excellent review given by Porter and Davis[3] Recent efforts have yielded even further successes.[4–6] However, a common denominator in most reported results is that the high temperature aging was performed in inert ambient or vacuum. Unless the goal of these efforts is to develop complex and expensive high temperature hermetic packaging to protect the contacts, the ultimate test of contact thermal stability should be performed in air. Thermally stable contacts obtained in air ambient would thus require less expensive and less complex packaging.

The result reported here is an evolution from earlier studies[7,8] based on the principle that reliability of contacts destined for high temperature applications could be better understood within the context of the overall thermochemical interactions between the multilayer metallization, the SiC material, and the outside environment. The need to preserve bondability (i.e., wire bond) between device and bond pads was also considered important. An effort to validate this strategy in a previous study used the Ti(100 nm)/$TaSi_2$(200 nm)/Pt(300 nm) metallization on *n*-type single crystal SiC epilayers.[7] However, the contact surface morphology of this metallization system deteriorated significantly after 250 h of heating in air at 600 °C. Scanning electron microscopy (SEM) revealed surface morphological features such as ''blisters'' and long-range film buckling that would be expected to adversely affect the integrity of the contacts in the long run.

In this present work, an in-depth reliability study was performed to identify the thickness combination of the multilayer metallization that would provide optimum long-term performance. In addition to Auger electron spectroscopy (AES) and SEM, transmission electron microscopy (TEM), current–voltage ($I-V$) measurements, and energy dispersive x-ray (EDX) were also performed. The dominant failure mechanisms were identified and overcome. Additionally, a high temperature ohmic contact figure of merit ($OCFM_T$) is introduced as a reliability benchmark.

II. EXPERIMENT

Two Si-face (0001)-oriented high resistivity *p*-type 6H– and 4H–SiC 50-mm-diam substrates 3.5° and 8° off axis, respectively, each with 2 μm *n*-type epilayers, were obtained from Cree, Inc.[9] The epilayer doping levels of the 6H– and

a)Electronic mail: robert.okojie@grc.nasa.gov

4H–SiC samples were 7×10^{18} and 2×10^{19} cm^{-3}, respectively. Samples measuring 1 cm^2 were cut from each substrate. Two samples from each polytype were then paired together to obtain two sample sets labeled A and B. All samples were initially treated in H_2SO_4 and H_2O_2 solution (Piranha clean) for 10 min, rinsed in de-ionized (DI) water, and blow dried in nitrogen. The samples were then dry oxidized at 1150 °C for 4 h, after which the oxide was stripped in 49% HF acid, rinsed in DI water, and blow dried again in nitrogen. The above procedure typically removes foreign elements including chlorine that reside on the surface and a few nanometers into the epilayer, thereby leaving a cleaner surface.[10] The samples then underwent a second dry oxidation at 1150 °C for 5 h. Sets of four straight-line equidistant circular via holes 30 μm in diameter were defined in photoresist by standard photolithography to expose the oxide, which was then etched in buffered HF for 1 min to expose the SiC epilayer. The photoresist was subsequently stripped in acetone. Following another Piranha clean, the samples were rinsed in DI water, blow dried with nitrogen, and transferred immediately into the metallization chamber. A 1 h heat treatment at 300 °C was performed under ultrahigh vacuum conditions ($\sim10^{-8}$ Torr) and the samples were allowed to cool prior to the multilayer metal deposition. The sputtering system, deposition process, and etching are fully described in previous work.[8] The metallization thickness combinations deposited on sample sets A and B were Ti(100 nm)/$TaSi_2$(200 nm)/Pt(300 nm) and Ti(100 nm)/$TaSi_2$(400 nm)/Pt(300 nm), respectively. After metal deposition, patterning, and etching, each of the four 1 cm^2 samples was diced into 12 pieces (now a total of 48 pieces), such that each piece contained at least one set of the four straight-line equidistant 30-μm-diam circular contacts to enable four-point probe measurements. Each piece then underwent a specific thermal treatment. The samples were evaluated at several stages: as deposited state, after an initial 30 min nitrogen anneal at 600 °C, and after treatments in air ambient at 600 °C at 100 h intervals up to 1000 h. At each 100 h interval or when necessary, the samples were cooled down and one piece of each polytype was selected for characterization via SEM, TEM (selectively), AES, and $I-V$ measurements. Calculation of the specific contact resistance (SCR) was based on Kuphals's modified four-point probe method.[11] In this case, however, we were more interested in the overall resistance change at the interface. Therefore, the resistances of the metal/alloy and alloy/SiC were lumped together and defined as the SCR. As a result, the SCR values were higher than the case if only the alloy/SiC resistance was considered.

In preparation for the cross-sectional transmission electron microscopy (XTEM) analysis, the SiC samples with the multilayer thin films were sectioned using a diamond saw, then two of the pieces were glued face to face with a degassed mixture of epoxy and sandwiched between two SiC dummy wafers. The sandwiched specimens were sliced to a size of 2.5 mm×2 mm×0.5 mm. One of the slices was thinned to electron transparency using a tripod to polish both sides and argon ion-beam milling for a short period of time. Diffraction contrast and high-resolution images, selected-area and microdiffraction data were recorded using a Philips™ CM200 TEM operating at 200 keV. The TEM is coupled to an EDAX™ energy dispersive x-ray spectrometer and a Gatan image filter using electron energy loss spectra for elemental analysis.

The AES system used for most of this work was a PHI-590™ scanning AES system with a single pass cylindrical mirror analyzer and a coaxial electron gun. The relative energy resolution of the analyzer was set at 0.6%. The electron beam energy was 3 keV and the beam current was approximately 4 μA. The incident angle of the electron beam with respect to the sample surface normal was 60°. A positive argon ion beam with 4 keV beam energy was used to obtain the AES depth profiles and was rastered over an area of about 1.5 mm×1.5 mm. Since the $TaSi_2$/Ti interface was found to be very stable in all the samples, with no significant Ta migration or reaction with the Ti layer, this interface was used to establish layer thickness in the heat-treated samples. AES analysis was also performed using a VG Instruments Microlab 310-F with a beam diameter <100 nm, which had much better spatial resolution than the PHI-590, thereby making it possible to perform spatial transition from the contact center to the contact edge. The sensitivity factors were configured to match the conditions of the previous analyses on the PHI-590.

III. RESULTS AND DISCUSSIONS

In the as-deposited state for both metallization schemes, the platinum layer exhibited multigrain texture as can be seen in the XTEM of Fig. 1(a). Also in the XTEM, the Ti/SiC interface is shown to be very abrupt, with the formation of pseudo-epitaxial titanium during sputter deposition. The AES depth profile of the as-deposited representative metallization is shown in Fig. 1(b). The sputter etch rate was calibrated to be 6.8 nm/min using a 100 nm TaO_2 film on Ta foil. However, the actual sputter rate was found to vary with each layer, i.e., the Pt layer sputtered much faster than the $TaSi_2$ and Ti layers.

After the initial 30 min anneal at 600 °C in N_2 ambient, the reaction products obtained in both metallization schemes at the reaction zones were generally similar, as shown in the AES depth profile of Fig. 2(a). Platinum silicide had formed on the topmost surface via the partial decomposition of $TaSi_2$. This silicide product functioned as a sacrificial diffusion barrier against oxygen diffusion to the metal/SiC interface. At the Ti/SiC reaction zone, XTEM analysis of Fig. 2(b) indicates the formation of titanium silicide as the reaction product in intimate contact with SiC.

A. Sample A: Ti(100 nm)/$TaSi_2$(200 nm)/Pt(300 nm)

For this metallization, the volume content of silicon in the $TaSi_2$ was determined by calculation so that the reaction products predicted can be described by the equation

$$6Pt + TaSi_2 \rightarrow 2Pt_3Si + Ta \tag{1a}$$

at the Pt/$TaSi_2$ zone, and

$$6Ti + 3SiC \rightarrow Ti_5Si_3 + TiC + 2C \tag{1b}$$

at the Ti/SiC zone.

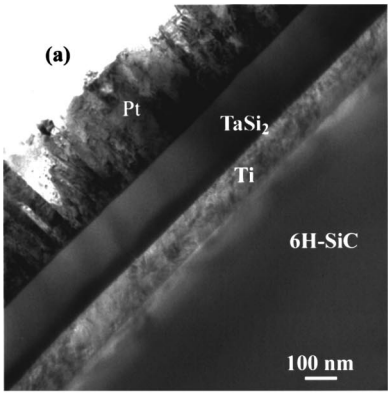

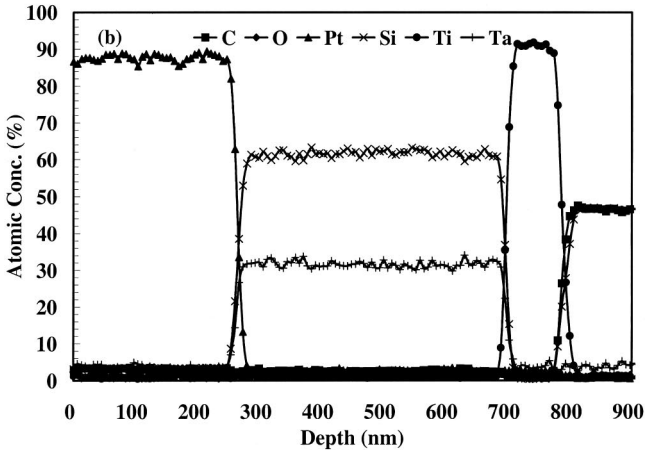

FIG. 1. The as-deposited Ti/$TaSi_2$/Pt metallization on 6H–SiC shown in (a) cross-sectional TEM reveals multigrain columns of platinum and pseudo-epitaxial titanium on SiC; (b) is the representative AES depth profile.

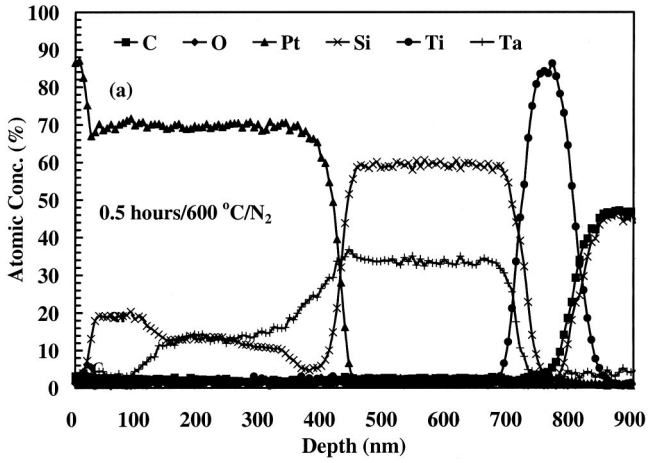

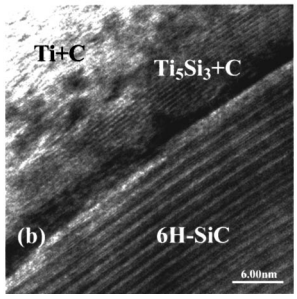

FIG. 2. After anneal in nitrogen for 30 min at 600 °C (a) AES depth profile of sample A, Ti(100 nm)/$TaSi_2$(200 nm)/Pt(300 nm), on SiC shows decomposition of $TaSi_2$ and the formation of platinum silicide as the new topmost layer; (b) cross-section TEM of SiC interface reveals an approximately 8 nm crystalline Ti_5Si_3 ($c \approx 0.55$ nm) as the new reaction product in contact with SiC.

The representative AES depth profile [Fig. 2(a)], however, indicates a 3.4:1 Pt:Si atomic ratio as opposed to the predicted 3:1 ratio for a thermodynamically stable form of Pt_3Si.[12] However, within limits of AES measurement sensitivity error, the reaction product agrees with Eq. (1a). From the AES depth profile, it was difficult to distinguish specific reaction products at the Ti/SiC zone. However, the XTEM image of Fig. 2(b) reveals crystalline titanium silicide with lattice constants close to Ti_5Si_3 ($a \sim 0.743$ nm, $c \sim 0.55$ nm),[13] as the reaction product in contact with SiC. There was only a small indication in Fig. 2(a) AES that titanium carbide formed after this initial 30 min anneal in nitrogen.

Upon initial heating of the annealed metallization layers in air, the platinum silicide on the surface reacts with oxygen to form a thin (40 nm), protective layer of SiO_2 on the surface of the contact. AES results indicate that the oxidation of the protective platinum silicide overlayer has a parabolic growth rate that significantly slows down further migration of oxygen to the SiC interface, thereby extending the life of the contact. It can be seen in the AES of Fig. 3 that by 200 h of heat treatment in air at 600 °C, excess Pt had reached the Ti_5Si_3 layer. The heat of formation of platinum silicide thermodynamically favors the reduction (i.e., decomposition) of titanium silicide[14] as was observed to have occurred. Very little increase in thickness of Ti_5Si_3 occurred at the SiC interface after this time, which was an indication of very slow reaction kinetics at the SiC interface due to the low diffusivity of titanium.[7] The carbon that was freed up at the SiC interface during this reaction migrated into the unreacted Ti region, where it had reacted to form a now discernable Ti_xC_y specie. Free titanium is observed to have migrated to the

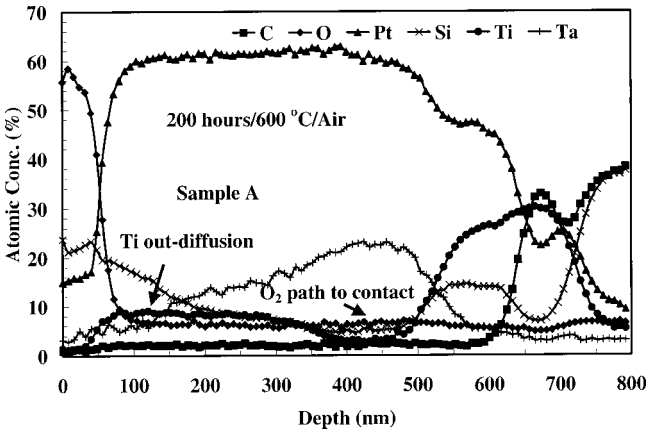

FIG. 3. AES depth profile of sample A, Ti(100 nm)/$TaSi_2$(200 nm)/Pt(300 nm), on SiC after 200 h of heat treatment at 600 °C in air. Decomposition of titanium silicide by platinum is observed and also indications of possible formation of platinum silicide at the SiC interface. Observed also is the migration of titanium toward the surface and diffusion of oxygen toward SiC.

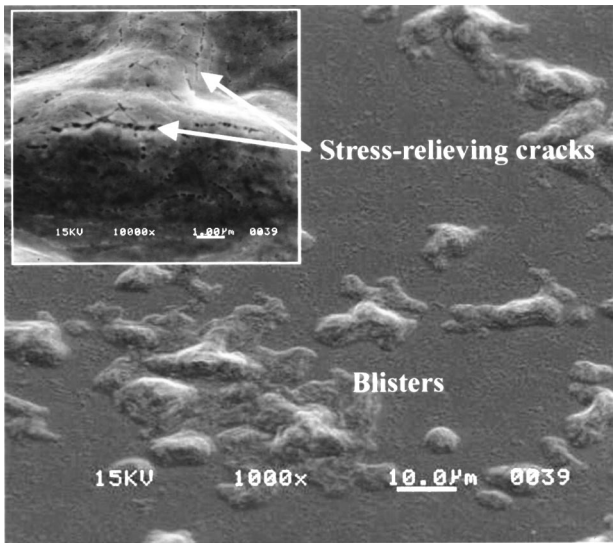

FIG. 4. SEM micrograph of sample A after heat treatment in air at 600 °C for 250 h reveals nonuniform oxide growth network on the surface manifested as blisters. Magnified inset of a blister reveals microcracks, likely a stress relief mechanism as a result of the local agglomeration of titanium under the platinum silicide.

surface and oxygen diffusing to the SiC interface. After 250 h, the free titanium had agglomerated locally at the platinum silicide subsurface, causing the formation of blisters seen in the SEM image of Fig. 4. The stress generated on the blisters was relieved by cracks that are clearly visible in the magnified inset in Fig. 4. These cracks possibly presented a diffusion path for oxygen to react with the titanium all the way to the SiC surface, as seen in Fig. 3. Surface analysis of the blisters by EDX revealed high platinum, silicon, and oxygen counts but very little of titanium, suggesting that out-diffusing titanium was indeed trapped at the subsurface of the platinum silicide layer.

B. Sample B: Ti(100 nm)/$TaSi_2$(400 nm)/Pt(300 nm)

The volume content of silicon in $TaSi_2$ was also calculated and verified by existing thermodynamic data[12] such that the reaction product could be described by the equation

$$4Pt + TaSi_2 \rightarrow 2Pt_2Si + Ta. \quad (2)$$

Figures 5(a) and 5(b) represent the AES depth profile and the SEM of the surface after heat treatment in air at 600 °C for 250 h, respectively. In sharp contrast to sample A after a lesser duration of 200 h at 600 °C in air (Fig. 3), the AES depth profile of sample B [Fig. 5(a)], shows the absence of titanium migration to the surface and also no oxygen diffusion to the contact. As a result, no blisters were formed on the surface, hence a smoother surface morphology as observed in the SEM image of Figure 5(b). This is in sharp contrast to the blister ridden surface of sample A (Fig. 4) after 200 h at 600 °C in air. In addition, and most importantly, the deleterious decomposition of titanium silicide by migrating platinum at the SiC reaction zone was prevented, thereby preserving the stability of that zone, with only very slow reaction kinetics between titanium and SiC.

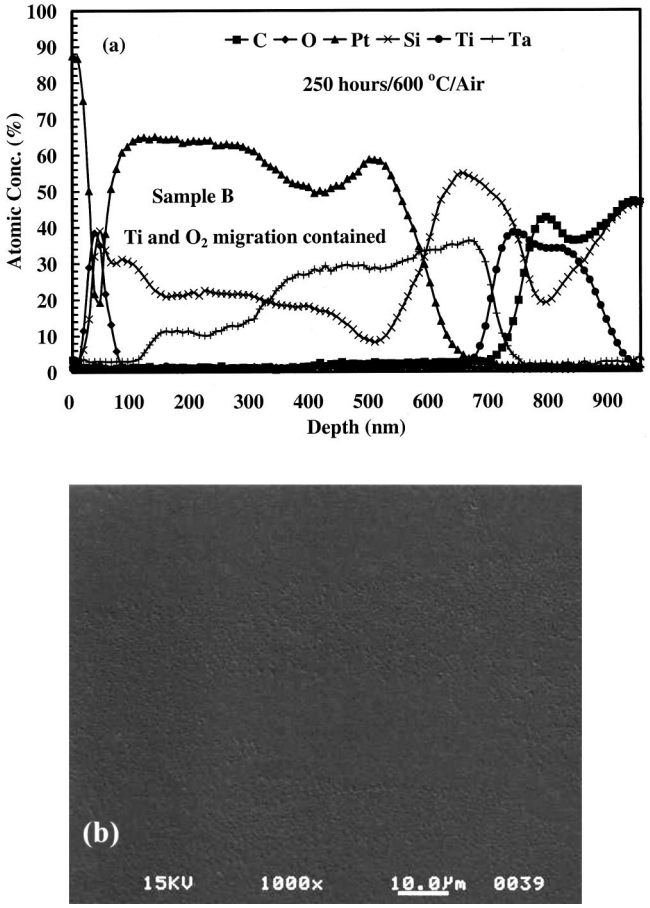

FIG. 5. After 250 h of heat treatment at 600 °C in air, (a) AES depth profile of sample B, Ti(100 nm)/$TaSi_2$(400 nm)/Pt(300 nm), shows the suppression of titanium out-diffusion and prevention of oxygen diffusion to SiC; (b) corresponding SEM micrograph depicting a smoother surface morphology in contrast to Fig. 4 of sample A.

From the above results, the metallization scheme B with smaller Pt/$TaSi_2$ volume ratio provided greater thermal stability to support stable contacts at 600 °C in air. The AES results of both samples clearly indicated the prevention of further penetration of oxygen into the contact due to the formation of a protective oxide layer on the platinum silicide. We have determined in previous work[7] that the reaction kinetic of platinum silicide has parabolic characteristics, which implies a very slow rate of oxidation of the platinum silicide, thereby inhibiting uncontrolled migration of oxygen to the SiC interface.

Having now understood the beneficial and destructive role of platinum in this system, for the actual electrical characterization, a new pair of 6H– and 4H–SiC samples were prepared in which the deposited platinum thickness was 200 nm while maintaining the Ti and $TaSi_2$ thickness of 100 and 400 nm, respectively. The room temperature $I-V$ plots for the 6H– and 4H–SiC samples after intermittent stages of heat treatments and cooling up to 1000 h at 600 °C in air are shown in Figs. 6(a) and 6(b), respectively. The $I-V$ plot of the as-deposited metallization on the 6H–SiC sample was fairly ohmic [Fig. 6(a)]. After annealing in nitrogen at 600 °C for 30 min, the slope of the $I-V$ curve decreased slightly relative to the as-deposited state, with SCR of 1.68

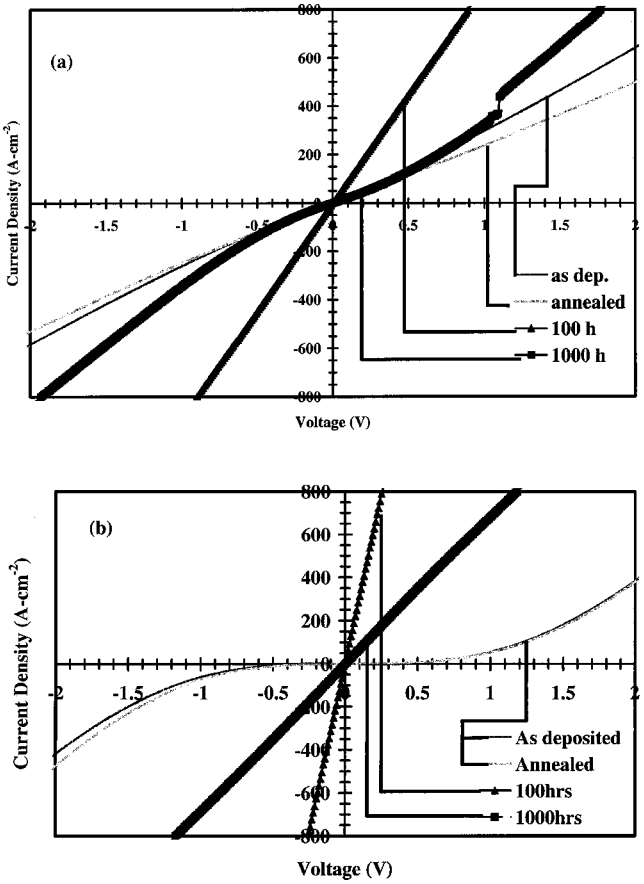

FIG. 6. Representative $I-V$ characteristic curves of the optimized Ti(100 nm)/$TaSi_2$(400 nm)/Pt(200 nm) taken after 1000 h of heat treatment and cooling down on (a) *n*-type 6H–SiC, (b) *n*-type 4H–SiC. The nonlinearity seen in (a) after 1000 h is attributed to lateral oxidation of the contact (Fig. 8), which may also have been responsible for changes in the $I-V$ slopes in both 6H– and 4H–SiC samples.

$\times 10^{-4}$ Ω cm^2 shown in Fig. 7. It also shows the SCRs for both polytypes, also calculated after every 100 h of heating at 600 °C in air and cooling down. However, after 100 h of heat treatment in air at 600 °C, the $I-V$ slope increased significantly with measured of 4.6×10^{-5} Ω cm^2. The nonlinear

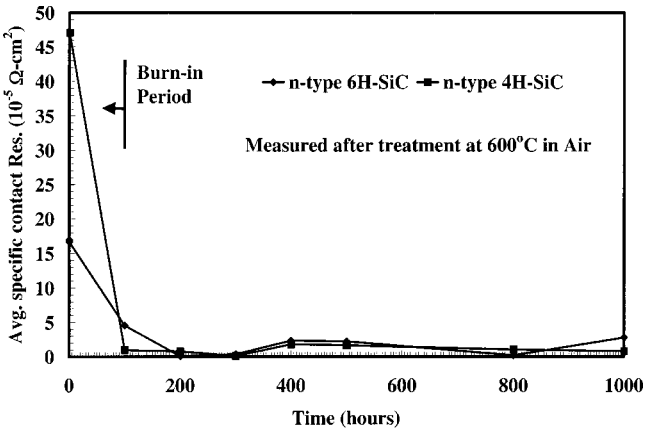

FIG. 7. The average specific contact resistivity of the optimized Ti(100 nm)/$TaSi_2$(400 nm)/Pt(200 nm) on the *n*-type 6H– and 4H–SiC at each 100 h cyclic heating at 600 °C and cooling down. The period within the first 100 h was for burn in to allow the dominant reactions to complete.

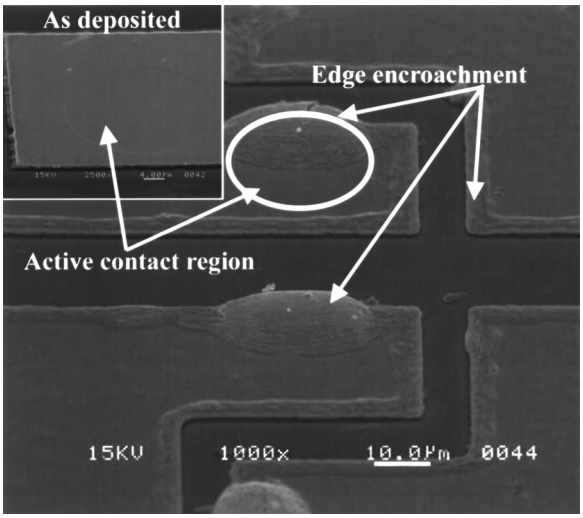

FIG. 8. SEM micrograph of Ti(100 nm)/$TaSi_2$(400 nm)/Pt(200 nm) shows a fairly smooth surface morphology when compared to the as-deposited metallization shown in inset. Edge encroachment to the electrically active circular contact region due to lateral oxidation is observed.

$I-V$ plot observed after 1000 h is explained below. In the case of the 4H–SiC sample, the trend was slightly different at the initial stage. The $I-V$ of the as-deposited metallization and after the initial 30 min nitrogen anneal was rectifying, despite its higher doping level than the 6H–SiC sample. This could be attributed to the higher density of surface states near the conduction band edge of 4H–SiC[15] that act as recombination centers for holes and electrons.[16] However, it became ohmic upon subsequent heat treatment in air with a relatively constant SCR similar to the 6H–SiC sample.

The initial high values of SCR on both polytypes within the first 100 h of heat treatment in air at 600 °C was attributed to ''burn-in'' period when the dominant reactions were incomplete. Therefore, the thermal stability was evaluated after the first 100 h when the SCR became lower. The variation in SCR values during the intermittent measurement was attributed to the previously noted oxide growth on the contact surface, which made probing of the underlying conductive platinum silicide difficult. To obtain a good electrical probe tip contact, the surface had to be scratched to break through the oxide, thus exposing the underlying conductive platinum silicide.

The condition of the contact surface after 1000 h at 600 °C in air is depicted in the SEM of Fig. 8, with the as-deposited metallization displayed in the inset for comparison. While the surface morphology within the electrically active circular contact region remained relatively smooth after 1000 h at 600 °C in air, lateral oxidation of the contact pads had caused delamination at the edges of the pads and subsequent encroachment into the active circular contact regions (Fig. 8). The nonlinear $I-V$ plot of the contact on 6H–SiC after 1000 h at 600 °C in air as seen in Fig. 6(a) was attributed to this undesirable edge encroachment into the active circular contact region. Very high concentrations of titanium and oxygen were observed on the delamination by EDX analysis after 1000 h. Also, AES profiling of the encroaching edge indicated extensive oxidation of the delami-

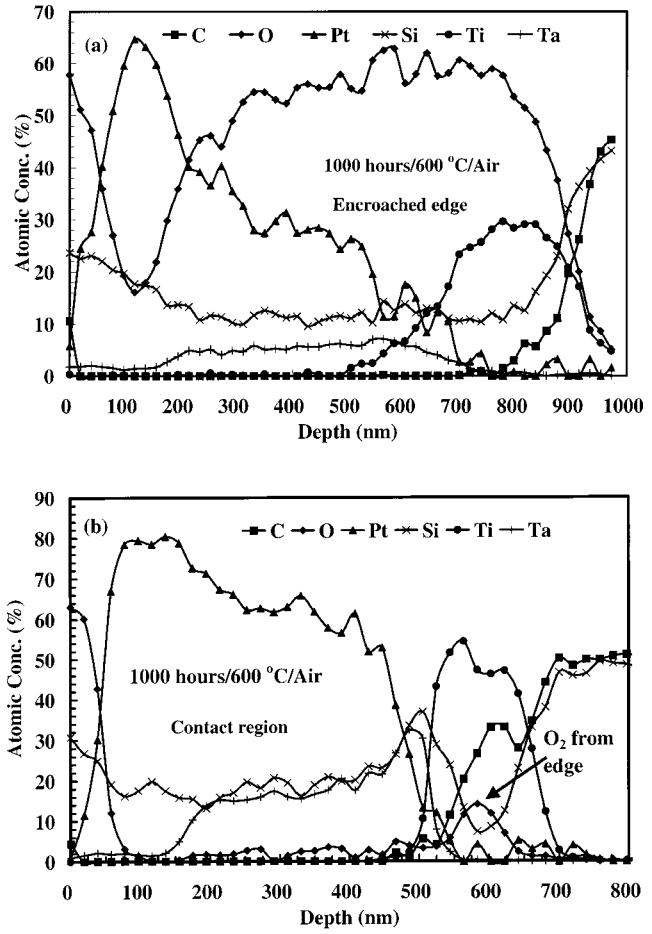

FIG. 9. AES depth profile of Ti(100 nm)/$TaSi_2$(400 nm)/Pt(200 nm) on SiC after 1000 h of heat treatment at 600 °C in air, (a) on the encroaching edge shows extensive oxidation of the metallization there, (b) on the active circular contact region shows no oxygen penetration from the top. The oxygen observed near the SiC reaction zone could only be from the edge, and not diffusion from the surface.

nation as shown in Fig. 9(a). However, AES depth profiling of the active contact region shown in Fig. 9(b) after 1000 h at 600 °C in air revealed no significant changes in the reaction products when compared against the AES profile of sample B after 250 h [Fig. 5(a)]. The oxygen observed near the SiC interface could only have migrated laterally from the edge as previously noted. The edge encroachment is believed to have occurred because the Shockley pads were not dielectrically passivated at the edges. In future device fabrication, dielectric passivation of the pads with silicon nitride will be incorporated.

C. New ohmic contact figure of merit

There is no previous reliability figure of merit for high temperature ohmic contacts to wide band gap devices. The figure of merit generally quoted is the specific contact resistance, which does not take into consideration the time duration of thermal treatments. Combining transient electrical characteristics and temperature effects of the contacts should provide crucial information about prevailing reaction kinetics and this can be utilized to predict the degree of thermal stability of the contact resistance. Therefore, a reliability number, $OCFM_T$, is empirically derived and expressed as

$$\mathrm{OCFM}_T=\frac{{}^{V}F_{2},t_{2}-{}^{V}F_{1},t_{1}}{J|\Delta t|}[\Omega\ \mathrm{cm}^2\ \mathrm{h}^{-1}], \tag{3}$$

where at a constant current density, J ($\mathrm{A\,cm^{-2}}$), V_{F2} (V) is the forward voltage at maximum time duration, t_2 (h); V_{F1} (V) is the forward voltage at minimum time duration, t_1 (h); and Δt is the difference between t_2 and t_1. Therefore, in an ideal case, a thermally stable ohmic contact would have an $OCFM_T$ of zero if at the fixed current density the forward voltage did not deviate with time at temperature. From the $I-V$ plots of Figs. 6(a) and 6(b), for $t_1=100$ h and $t_2=1000$ h, the $OCFM_{600\,^\circ C}$ for these contacts to the 6H–SiC and 4H–SiC was calculated to be 2.58×10^{-6} and $1.59\times10^{-6}\ \Omega\ \mathrm{cm^2\,h^{-1}}$ at a fixed current density of 800 $\mathrm{A\,cm^{-2}}$, respectively.

IV. CONCLUSION

Accurate prediction of dominant failure mechanisms in a multilayer metallization system is an arduous task due to the complex reaction kinetics associated with the process. However, this work attempted to validate a model of the effect of platinum on the overall integrity of the ohmic contact when subjected to open air heat treatment at 600 °C. From the above results, the following observations were made: In a high-platinum content silicide system, excess platinum appears to migrate and reduce stable compounds in a thermodynamically favorable reaction. The substitution of titanium silicide with platinum silicide as the new contact to SiC alters the electrical characteristics of the contact by increasing the SCR and/or degrading it mechanically. The out-diffusion of titanium to the surface facilitates undesirable oxygen migration toward the metal/SiC interface. The observed delamination on the contact surface is the result of stress induced by the uneven oxidation of the contact. Improved stability of the metallization system was obtained by understanding this relationship and reducing the platinum content.

While platinum is desired for the purpose of forming a protective silicide overlayer as the first line of defense against oxygen diffusion, it can also lead to contact degradation if not carefully controlled. Further improved understanding of the long-term reliability of the ohmic contact requires the performance of combined thermal and electrical stress analysis. Such analysis is fundamental because it could reveal new failure mechanisms such as electro-thermal migration, and/or electrical hotspots due to thermal gradient.

ACKNOWLEDGMENTS

The authors thank Dr. Jih-Fen Lei, Dr. Gary Hunter, Dr. Larry Matus, Dr. Mary Zeller, and Dr. Phil Neudeck for their technical reviews and support, and Drago Androjna for the SEM images. This work was funded by NASA under the Glennan Microsystems Initiative (GMI).

[1] C. E. Ryan, *Silicon Carbide*, Mat. Res. Bull., edited by H. K. Henisch and R. Roy (Pergamon, New York, 1969), Vol. 4, pp. S1–12.

[2] P. G. Neudeck, *The VLSI Handbook*, edited by Wai-Kai Chen (CRC Boca Raton, FL, 2000), Chap. 6, pp. 1–32.
[3] L. M. Porter and R. F. Davis, Mater. Sci. Eng., B **34**, 83 (1995).
[4] R. Wenzel, F. Goesmann, and R. Schmid-Fetzer, Proceedings of the High-Temperature Electronic Materials, Devices and Sensors Conference, San Diego, CA, 1998, pp. 159–164.
[5] S. Liu, K. Reinhardt, C. Severt, J. Scofield, M. Ramalingam, and C. Tunstall, Sr., Proceedings of the 3rd International High Temperature Electronics Conference, Alburquerque, NM, 1996 pp. VII (9–13) (1996).
[6] N. A. Papanicolaou, A. E. Edwards, M. V. Rao, A. E. Wickenden, D. D. Koleske, R. L. Henry, and W. T. Anderson, Proceedings of the 4th International High Temperature Electronics Conference, Albuquerque, NM, 1998, pp. 122–127.
[7] R. S. Okojie, D. Lukco, Y. L. Chen, D. Spry, and C. Salupo, *Mater. Res. Soc. Symp. Proc., Wide-Bandgap Electronic Devices*, edited by A. K. Agarwal, J. A. Cooper, Jr., E. Janzen, and M. Skowronski (Materials Research Society, Warrendale, PA, 2001), Vol. 640, pp. H7.5.1–6.
[8] R. S. Okojie, D. Spry, J. Krotine, C. Salupo, and D. R. Wheeler, *Mater Res. Soc. Symp. Proc., Wide-Bandgap Electronic Devices*, edited by R. J. Shul, F. Ren, M. Murakami, and W. Pletschen (Materials Research Society, Warrendale, PA, 2000), Vol. 622, pp. T8.3.1–6.
[9] Cree, Inc., Durham, NC 27703.
[10] R. S. Okojie, D. Lukco, and L. Keys, Technical Digest, International Conference on Silicon Carbide and Related Materials, Tsukuba, Japan, October 28–November 2, 2001, p. 416.
[11] E. Kuphal, Solid-State Electron. **24**, 69 (1981).
[12] *Alloy Phase Diagrams*, ASM Handbook, Vol. 3 (ASM International, Materials Park, OH, 1997), pp. 2–347.
[13] W. B. Pearson, *A Handbook of Lattice Spacings and Structures of Metals and Alloys*, (Pergamon, London, 1967), Vol. 2, p. 392.
[14] J. M. Andrews and J. C. Phillips, Phys. Rev. Lett. **35**, 56 (1975).
[15] N. S. Saks, S. S. Mani, and A. K. Agarwal, Appl. Phys. Lett. **76**, 2250 (2000).
[16] M. Shur, *Physics of Semiconductor Devices*, Prentice–Hall Series in Solid State Physical Electronics, edited by Nick Holonyak, Jr. (Prentice–Hall, Englewood Cliffs, NJ, 1990), p. 199.